ARTICLE

Chronic virus infection compromises memory bystander T cell function in an IL-6/STAT1-dependent manner

Isabel Barnstorf[1], Mariana Borsa[1]*, Nicolas Baumann[1]*, Katharina Pallmer[1]*, Alexander Yermanos[1], Nicole Joller[2], Roman Spörri[1], Suzanne P.M. Welten[1], Nike J. Kräutler[1], and Annette Oxenius[1]

Chronic viral infections are widespread among humans, with ∼8–12 chronic viral infections per individual, and there is epidemiological proof that these impair heterologous immunity. We studied the impact of chronic LCMV infection on the phenotype and function of memory bystander CD8^{+} T cells. Active chronic LCMV infection had a profound effect on total numbers, phenotype, and function of memory bystander T cells in mice. The phenotypic changes included up-regulation of markers commonly associated with effector and exhausted cells and were induced by IL-6 in a STAT1-dependent manner in the context of chronic virus infection. Furthermore, bystander CD8 T cell functions were reduced with respect to their ability to produce inflammatory cytokines and to undergo secondary expansion upon cognate antigen challenge with major cell-extrinsic contributions responsible for the diminished memory potential of bystander CD8^{+} T cells. These findings open new perspectives for immunity and vaccination during chronic viral infections.

Introduction

The immune responsiveness of a host toward microbial challenges or vaccines is given by the structural and cellular constituents of the immune system, which are subject to transient or permanent environmental modulations (Beura et al., 2016; Reese et al., 2016). Such modulations are a result of the previous infection and vaccination history of an individual, the constant encounter with commensal microorganisms on mucosal surfaces as well as the steady exposure to persistent viral infections. Chronic viral infections are highly prevalent, with ∼8–12 chronic infections per individual (Virgin et al., 2009).

Chronic viral infections can be subdivided into those caused by actively replicating virus, such as the infections caused by HIV and hepatitis B and C viruses in humans or lymphocytic choriomeningitis virus (LCMV) in the mouse, or latent/reactivating infections like the ones caused by herpesviruses. Over the past decades, substantial knowledge has been gained about the regulation of virus-specific T and B cell immunity in these types of persistent viral infections (Hangartner et al., 2006; Doria-Rose and Connors, 2009; Frebel et al., 2010; Wherry, 2011). In case of actively replicating persistent infections, virus-specific CD8^{+} T cell responses are generally compromised in size and function (termed T cell exhaustion; Wherry and

Kurachi, 2015), while virus-specific CD4^{+} T cells seem to preferentially differentiate into T follicular helper cells (Tfh; Fahey et al., 2011; Harker et al., 2011; Cubas et al., 2013). In addition, rapidly mutating viruses constantly change their recognition motifs and challenge antibody and T cell responses by immune evasion (Hangartner et al., 2006; Burton et al., 2012). In case of latent/reactivating persistent viral infections, substantial immune resources are devoted to the long-term control of viral reactivation events, most prominently seen in CMV infection in humans and mice. Here, impressively large expansions of CD8^{+} T cells are observed that bias the overall CD8 T cell pool durably toward an effector memory (T_{EM}) phenotype (Snyder, 2011; O'Hara et al., 2012; Klenerman and Oxenius, 2016).

These chronic viral infections affect immune responsiveness, e.g., by inducing and sustaining altered baseline levels of proinflammatory or immunomodulatory cytokines, by boosting innate immune responsiveness, and by changing the composition of lymphocyte populations as well as the function of APCs (Virgin et al., 2009). Indeed, substantial and sustained loss of "bystander" memory T cells was reported in chronic LCMV infection (Kim and Welsh, 2004), as well as impaired effector to memory transition of primed non–virus-specific CD8^{+} T cells

[1]Institute of Microbiology, ETH Zürich, Zürich, Switzerland; [2]Institute of Experimental Immunology, University of Zürich, Zürich, Switzerland.

*M. Borsa, N. Baumann, and K. Pallmer contributed equally to this paper; Correspondence to Annette Oxenius: aoxenius@micro.biol.ethz.ch.

(Stelekati et al., 2014). Also, in the context of HIV-1 infection, bystander T cells acquired an activated phenotype in individuals stopping antiretroviral therapy and hence experiencing viral rebound (Bastidas et al., 2014). Thus, thorough investigations on how specific persistent viral infections change immune responsiveness are of considerable importance, not only in the context of how persistent viruses affect immune homeostasis but also for predicting vaccine responsiveness or immune competence to control heterologous infections.

Here, we assessed the consequences of active chronic LCMV infection on existing heterologous immunity (memory bystander T cells). Chronic LCMV infection substantially reduced total numbers of existing heterologous memory CD8+ T cells through a mechanism that was partially dependent on perforin-mediated cytotoxicity, leading to disruption of splenic microarchitecture and hence survival niches. In functional terms, bystander memory CD8+ T cells exhibited a reduced capacity to produce inflammatory cytokines such as IFNγ and TNF. Phenotypically, bystander memory CD8+ T cells acquired a cell surface marker expression profile reminiscent of effector/exhausted cells, largely induced by IL-6. Transcriptional profiling of bystander memory cells corroborated the acquisition of exhausted signatures and revealed a gene expression profile induced by inflammatory cytokines rather than TCR triggering. Moreover, chronic virus infection negatively impacted the secondary expansion of memory bystanders upon challenge within chronically infected hosts. However, upon isolation of bystander memory T cells from an infected host and transfer into a naive environment, they resumed their memory potential. This indicates a superior role of the chronically infected host environment in restricting the functional capacities of bystander memory CD8+ T cells rather than durable cell-intrinsic functional alterations of memory bystander CD8+ T cells.

Results

Chronic virus infection significantly reduces total numbers of memory bystander T cells

To investigate the impact of chronic virus infection on memory bystander CD8+ T cells, we adoptively transferred naive CD45.1+ TCR-transgenic, OVA$_{257-264}$-specific (OT-I) CD8+ T cells into congenic CD45.2 WT C57BL/6 mice and generated OT-I memory cells by infection with recombinant vaccinia virus expressing OVA (VV-OVA). At least 30 d after infection, after an OVA-specific memory T cell pool had been established, mice were infected with either an intermediate or high dose of LCMV docile, leading to protracted infection with different rates of control (the intermediate dose is cleared by day 30 after infection, whereas a high-dose infection results in a chronic infection lasting until approximately day 300 after infection; Fig. 1, A and B). At 30 d after LCMV infection, the absolute number of memory OT-I T cells was strongly reduced upon chronic LCMV infection in spleen, lung, and blood. This effect was most pronounced upon a high-dose LCMV infection (Fig. 1 C).

To investigate whether this numeric reduction was due to an actively replicating chronic virus infection, we performed the same experiment using murine CMV (MCMV) instead of LCMV.

MCMV is a β herpes virus that, after control of lytic replication, persists in a latent form with recurrent episodes of reactivation. MCMV infection also leads to a significant reduction in memory bystander T cells in different organs (Fig. S1 A). We therefore tested whether this effect was exclusively true for chronic virus infection by infecting mice harboring memory bystander T cells with 200 focus-forming units (ffu) of the LCMV WE strain in order to cause an acute virus infection (Fig. S1 B). Interestingly, acute virus infection reduced total numbers of memory bystander T cells to a lesser extent than chronic virus infection (Fig. S1 B). These data highlight a common effect of chronic virus infections with an active replication or alternate stages of reactivation and latency on significant reduction in total numbers of memory bystander T cells in secondary lymphatic and peripheral organs.

Loss of memory bystander T cells is partially due to perforin-mediated cytotoxicity

To investigate whether this numeric reduction of memory bystander T cells by chronic virus infections was due to compromised survival niches in secondary lymphoid organs, for instance, by perforin-mediated destruction of T cell zone stromal structures by CD8+ T cells, we sorted memory bystander OT-I T cells ≥30 d after VV-OVA infection, transferred them in equal numbers either into WT or perforin-deficient (PKOB−/−) mice and infected the mice 1 d after transfer with LCMV docile (Fig. 2 A). At day 10 after infection, total numbers of the memory bystander T cells in the spleen and in the lung of WT recipients were reduced 17- and 7-fold, respectively. In contrast, this numeric reduction was significantly less pronounced (threefold in spleen and lung) in PKOB−/− mice upon chronic LCMV infection (Fig. 2 B). Interestingly, the memory bystander T cells in WT mice significantly down-regulated IL-7Rα expression upon LCMV infection in the spleen and in the lung, which could explain diminished survival due to reduced sensing of IL-7. The decreased expression of IL-7Rα was not observed in the absence of perforin upon LCMV infection (Fig. 2 B). To compare secondary lymphoid organ integrity in the presence or absence of perforin, and in particular the localization of T cells, we analyzed spleen sections of infected and uninfected WT or PKOB−/− mice by fluorescence microscopy. In uninfected mice, T cells reside in podoplanin-positive T cell zones, surrounded by the B cell zone (Fig. 2 C). Upon LCMV infection, T cells were mostly found outside podoplanin-positive T cell zones, and this spatial separation was far less pronounced in LCMV-infected PKOB−/− mice.

To quantify T cell localization within podoplanin-positive T cell zones, we selected a region of interest (ROI) based on podoplanin staining, measured the volume of CD3 and podoplanin stainings, and calculated the ratio of volume of CD3 to volume of podoplanin per ROI. This ratio was significantly reduced in WT mice upon LCMV infection, whereas this was not the case in the absence of perforin (Fig. 2 D), even though the volume of podoplanin per ROI was comparable among all groups (Fig. 2 D, bottom graph). Since the absence of perforin did not fully restore total numbers of memory bystander T cells, we further tested a potential involvement of natural killer (NK) cells and virus-specific effector CD8+ T cells (Fig. S1 D). The depletion
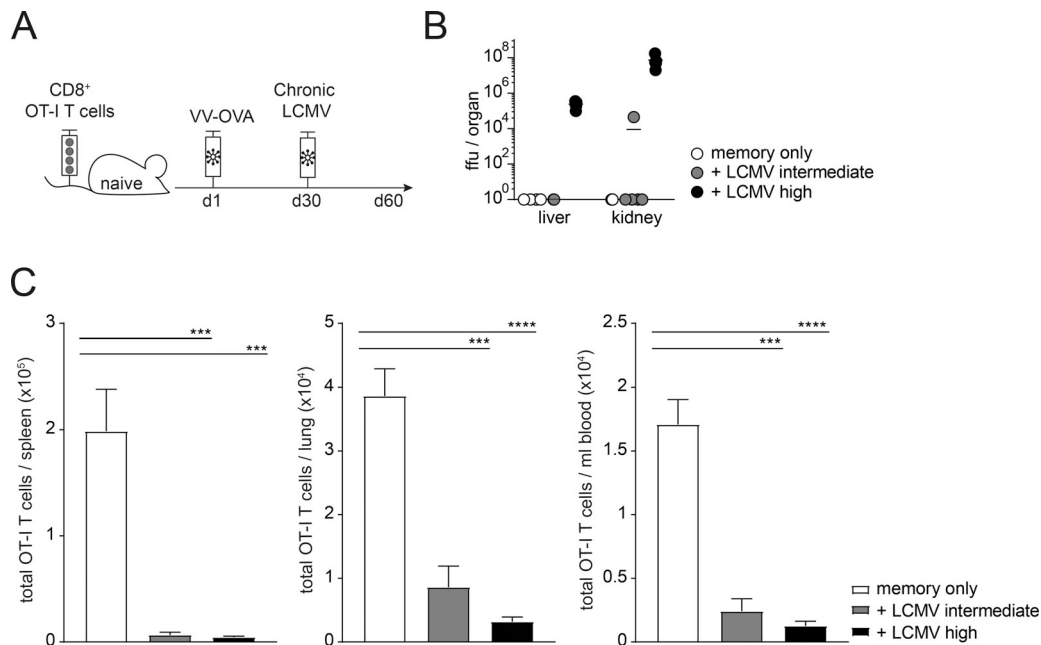
Figure 1. **Chronic virus infection significantly reduces total numbers of memory bystander T cells. (A)** Experimental approach. Adoptive transfer of CD45.1^{+} TCR-transgenic OVA$_{257-264}$-specific (OT-I) CD8^{+} T cells into congenic CD45.2 WT C57BL/6 mice, followed by priming with VV-OVA. On day 30 after priming, mice were infected with the persistent docile strain of LCMV with an intermediate (10^4 ffu) or high (10^6 ffu) dose. The experiment was terminated 30 d after LCMV infection. **(B)** Viral titers in liver and kidney at day 30 after infection. **(C)** Total cell counts of OT-I memory bystander CD8^{+} T cells in spleen, lung, and blood of memory only (white, no LCMV infection), memory + LCMV intermediate dose (gray), and memory + LCMV high-dose (black) 30 d after infection. **(B and C)** One representative experiment out of two is shown with four to five mice per group. Statistical analysis was performed using the unpaired two-tailed Student's t test: *, $P < 0.05$; ***, $P < 0.001$; ****, $P < 0.0001$. Error bars show SEM.

of NK cells had no effect on reduced memory bystander numbers (Fig. S1 D), whereas the presence of virus-specific effector CD8^{+} T cells did slightly reduce total numbers of memory bystander T cells (Fig. S1 E). These findings indicate that the loss of memory bystander T cells upon chronic LCMV infection is to a significant extent caused by perforin-mediated cytotoxicity and resultant disruption of splenic microarchitecture.

Chronic virus infection skews memory bystander phenotype and function

To examine the impact of a chronic virus infection on the phenotype and function of memory bystander T cells, we transferred CD45.1^{+} OT-I CD8^{+} T cells into congenic CD45.2^{+} WT C57BL/6 mice, followed by priming with VV-OVA. At least 30 d after priming, the mice were infected with intermediate- or high-dose LCMV docile. The memory bystander OT-I T cells were phenotypically and functionally analyzed 30 d after LCMV infection (Fig. 3 A). At this time point (60 d after VV-OVA infection), memory CD8^{+} T cells typically express high levels of IL-7Rα and very low levels of KLRG1. However, in LCMV-infected mice the expression of IL-7Rα was severely reduced on the memory bystander T cells compared to controls. In addition, the proportion of KLRG1^{+} cells was markedly increased, suggesting a conversion of the memory phenotype to more of an effector phenotype, or a selective loss of the IL-7Rα[+] compartment in the presence of chronic LCMV infection (Fig. 3 B). Interestingly, there was a correlation between phenotype and viral dose, with a higher percentage of KLRG1^{+} IL-7Rα[−] bystander memory OT-I

T cells in mice infected with a high dose of LCMV docile in comparison to intermediate-dose infection. Importantly, these phenotypic changes were not caused by cross-reactivity between the OT-I TCR and LCMV antigens (Fig. S2 A). To further exclude the possibility that this phenomenon is due to "antigen-specific" activation of the bystander CD8^{+} T cells facilitated by the expression of a second TCR α chain, we analyzed CD8^{+} OT-I bystander T cells from Rag1^{−/−} mice (Fig. S2 D). Comparable phenotypic changes were observed in RAG1^{+/+} and RAG1^{−/−} OT-I memory bystander cells, excluding a role of endogenous α chains that might confer LCMV reactivity to the OT-I T cells.

The phenotypical changes on memory bystander OT-I cells were exclusively induced by chronic and not by acute virus infection (Fig. S2 B). Moreover, IL-2, TNFα, and IFNγ cytokine production after in vitro restimulation with cognate antigen was significantly reduced in memory bystander T cells that were exposed to a chronic LCMV infection as compared with uninfected controls (Fig. 3 C). Of note, similar phenotypical, functional, and numeric alterations were also observed when fully formed memory bystander OT-I CD8^{+} T cells were adoptively transferred into recipients with already established chronic LCMV infection at 30 d after transfer (Fig. 3 D and Fig. S2 C).

Since chronic LCMV infection had a significant impact on the functionality of memory bystander T cells with respect to their ability to produce effector cytokines after restimulation, we further characterized these cells for expression of the co-inhibitory receptor PD-1 and the exhaustion marker CD39
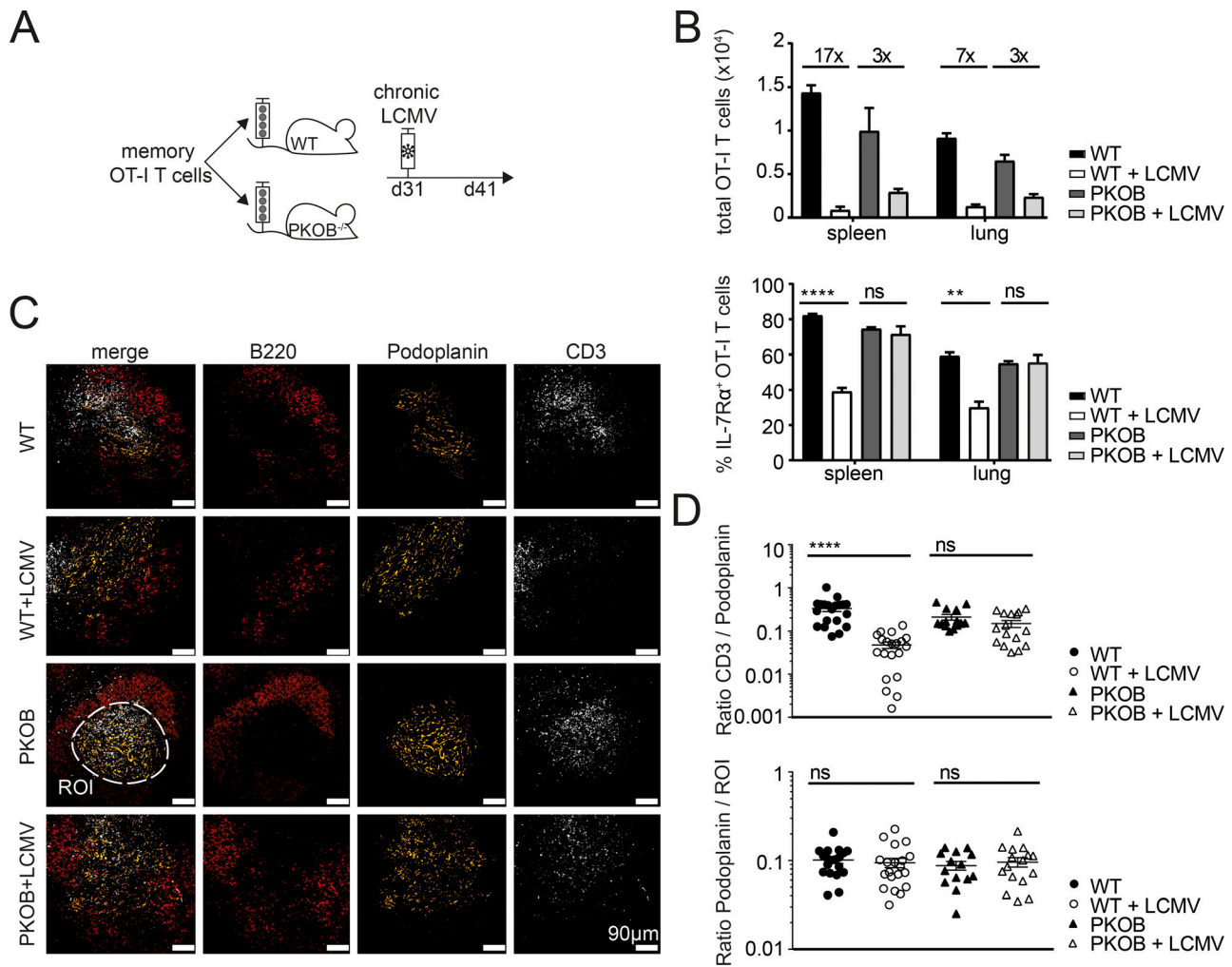
Figure 2. Loss of memory bystander T cells partially due to perforin-mediated cytotoxicity. (A) Experimental approach. Adoptive transfer of CD45.1^{+} OT-I memory CD8^{+} T cells (≥30 d after VV-OVA infection) into congenic CD45.2 WT C57BL/6 or PKOB^{−/−} mice. Mice were infected with LCMV docile 1 d after transfer. The experiment was terminated 10 d after LCMV infection. **(B)** Top: Total cell counts of OT-I memory bystander CD8^{+} T cells in spleen and lung of memory only in WT (black, uninfected), memory + LCMV in WT (white), memory only in PKOB^{−/−} (dark gray, uninfected), and memory + LCMV in PKOB^{−/−} (light gray). Bottom: Quantification of IL-7Rα[+] OT-I T cell percentages in spleen and lung of memory only in WT (black, uninfected), memory + LCMV in WT (white), memory only in PKOB^{−/−} (dark gray, uninfected), and memory + LCMV in PKOB^{−/−} (light gray). One representative experiment out of two with four mice per group is shown. Statistical analysis was performed using the unpaired two-tailed Student's t test: ns, $P \geq 0.05$; **, $P < 0.01$; ****, $P < 0.0001$. **(C)** Immunofluorescence staining of splenic thin sections of WT (top row), WT+LCMV (second row from top), PKOB^{−/−} (third row from top), or PKOB^{−/−} + LCMV (bottom row) for B cell zone (B220^{+}, red), T cell zone (podoplanin, yellow), and T cells (CD3^{+}, white). Scale bar, 90 μm. ROI, dashed white line. **(D)** Top: Ratio of volume of CD3 to volume of podoplanin in the ROI. 20 ROIs were analyzed per group. Bottom: Ratio of volume of podoplanin per ROI. Twenty ROIs were analyzed per group. Error bars show SEM.

([Gupta et al., 2015](#)). Interestingly, the memory bystander T cells expressed significantly higher levels of PD-1 exclusively upon chronic LCMV but not upon acute LCMV infection (Fig. S2 E). Additionally, bystander OT-I T cells coexpressed CD39 (Fig. S2 F), a marker that is typically expressed on exhausted CD8^{+} T cells and identifies CD8^{+} T cells with impaired function ([Gupta et al., 2015](#)). Thus, chronic viral infection, in contrast to resolved viral infection, significantly alters the phenotype and function of CD8^{+} memory bystander T cells.

KLRG1^{+} population arises from the IL-7Rα^{low} compartment

Next, we addressed the question whether the KLRG1^{+} IL-7Rα^{−} phenotype was the result of a phenotypical conversion or of a selective loss of the KLRG1^{−} IL-7Rα^{+} bystander CD8^{+} T cells in the setting of chronic LCMV infection. We therefore sorted memory OT-I cells with either low or high levels of IL-7Rα expression and transferred equal numbers into naive C57BL/6 mice, followed 1 d later by chronic LCMV infection. The phenotype of the memory bystander subsets was analyzed 2 wk after infection ([Fig. 4 A](#)). As depicted in [Fig. 4 B](#), the memory bystander T cells from the IL-7Rα[low] subset significantly up-regulated KLRG1 upon LCMV infection in the spleen and the lung, whereas the IL-7Rα[high] subset did not up-regulate KLRG1, indicating that chronic LCMV infection induces a conversion of the phenotype of the IL-7Rα[low] subset to a KLRG1^{+} phenotype.
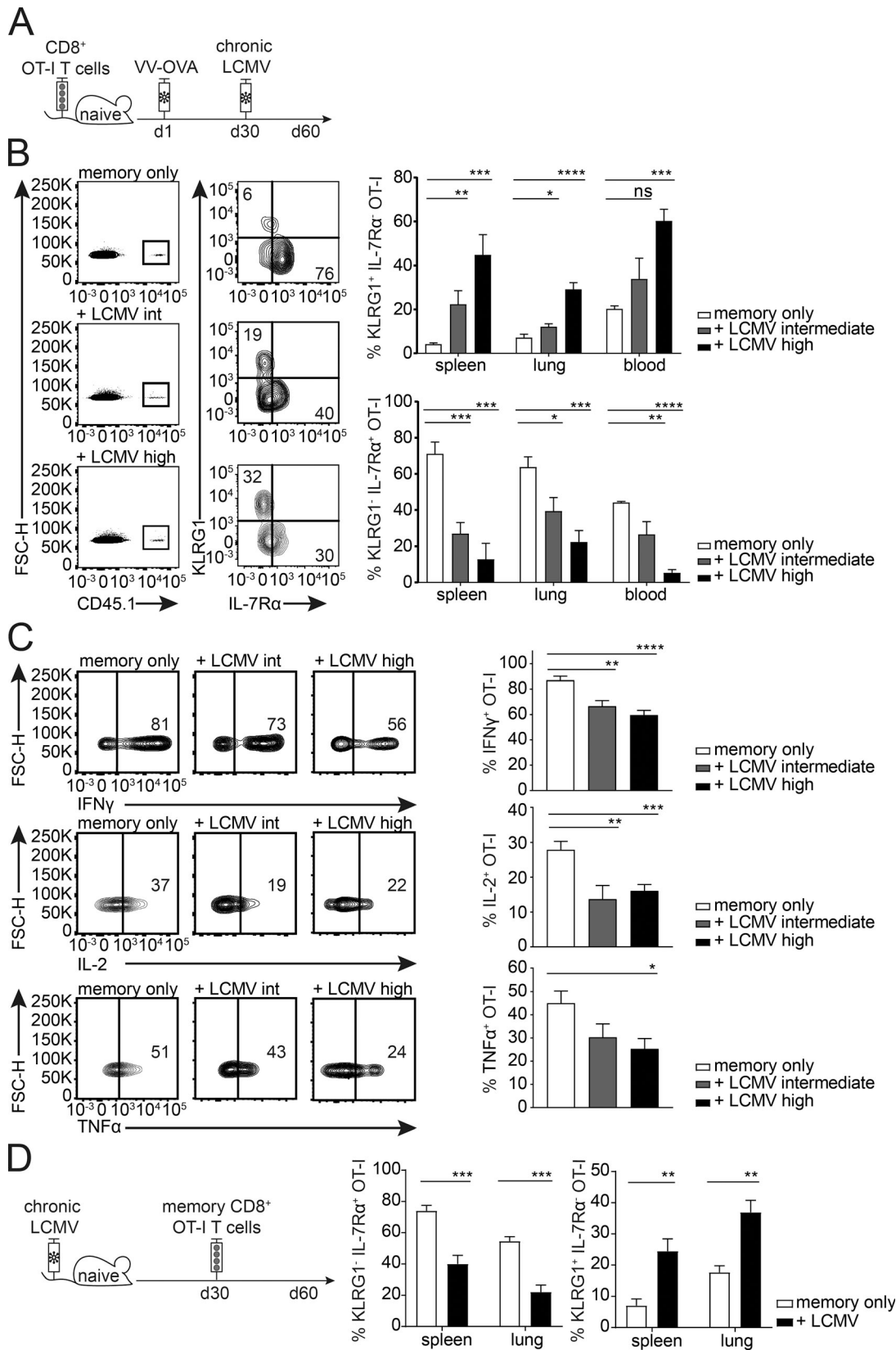
Figure 3. **Chronic virus infection skews memory bystander phenotype and function. (A)** Experimental approach. Adoptive transfer of CD45.1⁺ OT-I CD8⁺ T cells into congenic CD45.2 WT C57BL/6 mice, followed by priming with VV-OVA. On at least day 30 after priming, the mice were infected with LCMV docile at an intermediate (10⁴ ffu) or high (10⁶ ffu) dose. The experiment was terminated 30 d after LCMV infection. **(B)** Memory bystander CD8⁺ T cells in the spleen, lung, and blood. Flow cytometry plots pregated on live CD8⁺ T cells from spleen are depicted. Representative FACS plots are shown for CD45.1⁺ bystander

T cells (memory only, + LCMV intermediate, and + LCMV high) and their expression of KLRG1 and IL-7Rα. Right: Quantification of percentages of KLRG1+ IL-7Rα− OT-I T cells and KLRG1− IL-7Rα+ OT-I T cells shown for memory only (white, uninfected), + LCMV intermediate dose (gray), and + LCMV high dose (black) in the spleen and lung. FSC-H, forward scatter height. **(C)** Representative flow cytometry plots of cytokine production and quantification of IFNγ, IL-2, and TNFα production by memory bystanders from memory only (white, uninfected), + LCMV intermediate dose (gray), and + LCMV high dose (black) in the lung after 6 h of restimulation with the cognate antigen. **(D)** Left: Experimental approach. Mice were infected with a high-dose LCMV docile. 30 d after infection, memory bystander CD8+ T cells were adoptively transferred into chronically infected mice. Bystander T cells were analyzed 30 d after transfer. Right: Quantification of percentages of KLRG1+ IL-7Rα− OT-I T cells and KLRG1− IL-7Rα+ OT-I T cells shown for memory only (white, uninfected) and + LCMV (black) in the spleen and lung. **(B–D)** One representative experiment out of two is shown with four mice per group. Statistical analysis was performed using the unpaired two-tailed Student's *t* test: ns, P ≥ 0.05; *, P < 0.05; **, P < 0.01; ***, P < 0.001; ****, P < 0.0001. Error bars show SEM.

Transcriptional profile of memory bystander CD8 T cells induced by chronic virus infection

To investigate the molecular cues triggering these phenotypical changes in memory bystander cells during chronic LCMV infection, we analyzed gene expression profiles of OT-I memory cells that had or had not been exposed to chronic LCMV infection by RNA sequencing (RNA-seq). The transcriptional profile of the bystander T cells that were exposed to chronic LCMV infection (+LCMV) was distinct from the uninfected memory control (memory; Fig. 5 A). Comparing the expression profiles of genes associated with T cell differentiation revealed an up-regulation of genes encoding coinhibitory molecules such as CD39, PD-1, Tim-3, CTLA-4, 2B4, and TIGIT and down-regulation of IL-7Rα, CD62L, and CD44 (Fig. 5 B), which is in line with the flow cytometry data showing a more exhausted phenotype of the memory bystander T cells upon chronic virus infection. The transcriptional signatures revealed a robust up-regulation of inflammatory cytokines such as IL-6, IL-21, IL-1α, and IL-1β upon chronic LCMV infection, but also a down-regulation of T cell effector cytokines and molecules such as perforin, IFNγ, and granzyme B compared with memory bystanders that had not been exposed to chronic virus infection. The expression of transcription factors associated with memory formation or

maintenance shows that T-bet, which is highly expressed in effector CD8+ T cells and declines in its expression upon memory formation (Kaech and Cui, 2012), is down-regulated upon exposure to chronic virus infection. Strikingly, Tcf1, which is usually expressed in long-lived memory T cells (Sarkar et al., 2008; Kaech and Cui, 2012), is down-regulated. The down-regulation of Foxo1 also indicates that the bystander T cells exposed to chronic LCMV have an altered memory gene expression profile. Thus, the transcriptional profile of memory bystanders that were exposed to chronic virus infection versus controls reveals features of exhausted, and to some extent also "effector-like," cells. To elucidate which cell type they resemble more, we compared the transcriptional profile of LCMV-exposed bystander cells with differential gene expression profiles between effector LCMV-specific CD8+ T cells and memory T cells (Fig. 5 C, left) and between exhausted LCMV-specific CD8+ T cells and memory T cells (Fig. 5 C, right; Wherry et al., 2007). Red points correspond to those genes reported as up-regulated in the effector T cell gene set (Fig. 5 C, left) or exhausted T cell gene set (Fig. 5 C, right), whereas blue points correspond to those genes reported as down-regulated in the effector T cell gene set (Fig. 5 C, left) or exhausted T cell gene set (Fig. 5 C, right). This analysis revealed that the memory bystander T cells that were exposed to
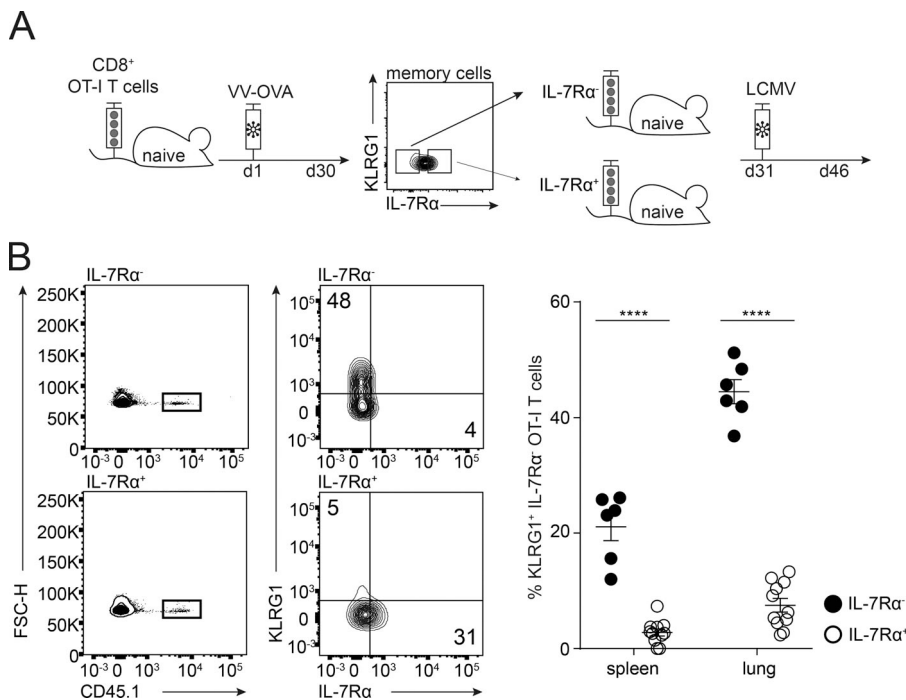

Figure 4. KLRG1+ population arises from the IL-7Rα^low compartment. (A) Experimental approach. Adoptive transfer of CD45.1+ OT-I CD8+ T cells into congenic CD45.2 WT C57BL/6 mice, followed by priming with VV-OVA. On day 30 after priming, OT-I memory cells were sorted for KLRG1− IL-7Rα^low and KLRG1− IL-7Rα^high and adoptively transferred into age- and sex-matched naive mice. 1 d after transfer, mice were chronically infected with LCMV docile. The experiment was terminated 15 d after LCMV infection. **(B)** Memory bystander CD8+ T cells in spleen and lung. Left: Flow cytometry plots pregated on live CD8+ T cells are shown. Representative FACS plots for CD45.1+ memory only and memory + LCMV and their expression of KLRG1 and IL-7Rα. Right: Quantification of percentages of KLRG1+ IL-7Rα− OT-I T cells are shown for IL-7Rα+ (white) and IL-7Rα− (black) in the spleen and lung. FSC-H, forward scatter height. One representative experiment out of two is shown with five mice per group. Statistical analysis was performed using the unpaired two-tailed Student's *t* test: *, P < 0.05; ****, P < 0.0001. Error bars show SEM.
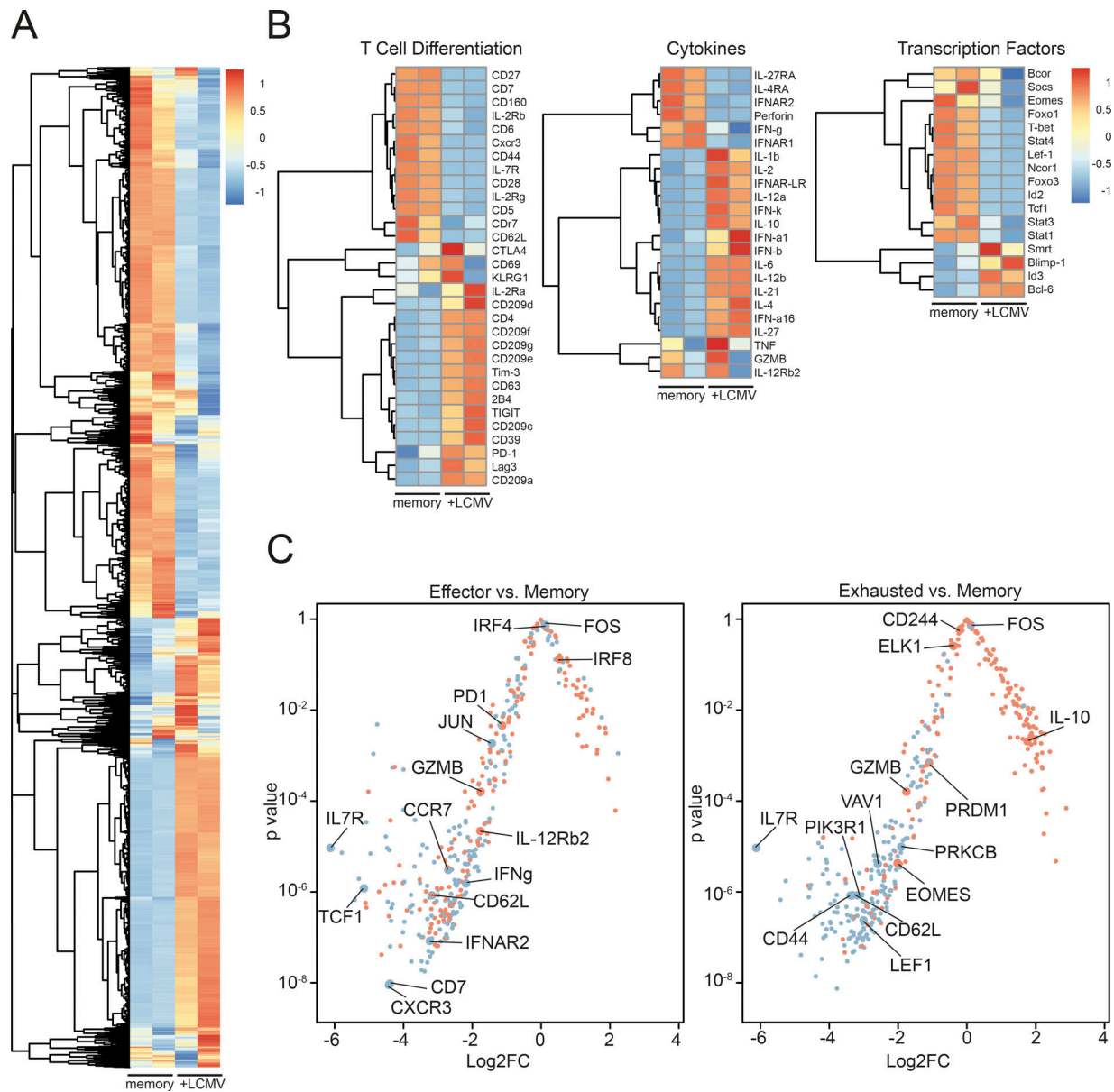
Figure 5. **Transcriptional profile of memory bystander CD8⁺ T cells induced by chronic virus infection. (A)** Heat map of differentially expressed genes comparing memory only (memory, uninfected) and memory + LCMV (+LCMV) infection. **(B)** Heat maps for selected genes of interest separated into categories of T cell differentiation, cytokines, and transcription factors comparing memory only (memory, uninfected) and memory + LCMV (+LCMV) infection. **(C)** Log2 fold change (Log2FC) and accompanying P values are shown for genes reported in four gene sets (Wherry et al., 2007). Red points correspond to those genes reported as up-regulated in the effector T cell gene set (left) or exhausted T cell gene set (right), whereas blue points correspond to those genes reported as down-regulated in the effector T cell gene set (left) or exhausted T cell gene set (right).

a chronic virus infection more closely resemble exhausted LCMV-specific CD8⁺ T cells, since 181 of 184 down-regulated genes and 100 of 182 up-regulated genes in exhausted CD8⁺ T cells were matching with our dataset. The comparison to the effector versus memory dataset revealed 168 matches of 187 down-regulated genes but only 43 matches of 184 up-regulated genes (Fig. 5 C).

Functionally, we had no indication that the OT-I bystander memory cells were activated by chronic LCMV infection in a TCR-dependent manner. However, to confirm these findings, we compared gene expression profiles associated with the TCR

signaling pathway between memory OT-I cells that were or were not exposed to LCMV and found a robust down-regulation of TCR signaling pathway–associated genes upon LCMV exposure (Fig. S3 A). Since LCMV infection is characterized by a strong and sustained induction of type I IFNs, we focused on the gene signatures of IFN-stimulated genes and observed a mix of up-regulated and down-regulated genes (Fig. S3 B).

In summary, the transcriptional analysis of bystander memory T cells revealed a profound change toward a more exhausted than effector-like gene expression signature during chronic virus infection. Based on the absence of signatures

associated with TCR signaling pathways, we assumed that these changes are mainly caused by the inflammatory cytokine milieu rather than by antigenic triggering.

IL-6 drives phenotypic alterations of memory bystander T cells

The robust enrichment of cytokine-related genes in memory bystander CD8+ T cells in the presence of a chronic virus infection led us to examine whether a specific cytokine might be responsible for the observed phenotypical changes. We therefore determined the phosphorylation status of different STAT proteins directly ex vivo and observed a strong pSTAT1 signature in the memory bystander T cells upon LCMV infection under viremic conditions (Fig. S4 A). Additionally, we performed a cytometric bead array (CBA) for IL-6, IFNγ, and TNF, as well as a bioassay for type I IFNs, comparing naive mice with LCMV-infected hosts. Interestingly, TNF and IL-6 levels were significantly elevated in the serum (Fig. 6 A) and the spleen and the lung (Fig. S4 C) even 30 d after LCMV infection. Since type I IFNs play a major role during LCMV infection and signal via STAT1, we blocked the type I IFN receptor (IFNAR) with a blocking antibody >2 wk during chronic LCMV infection and compared numeric and phenotypic changes of bystander OT-I memory CD8+ T cells in the presence or absence of IFNAR blocking antibodies. Surprisingly, blocking of IFNAR did not affect the typical phenotypic changes imposed by chronic bystander LCMV infection, nor did it rescue the attrition of memory bystander cells (Fig. S4 D), despite abrogation of the ex vivo STAT1 phosphorylation (Fig. S4 B). Neutralization of other cytokines associated with STAT1 signaling like IL-7, IL-2, and IFNγ did also not have an impact on the number or phenotype of memory bystander T cells upon LCMV infection (Fig. S4 E). Since the RNA-seq data and serum cytokine levels revealed IL-6 as a possible candidate and since IL-6 is known to signal via STAT1 and STAT3, we next blocked the IL-6R from the onset of LCMV infection (Fig. 6 B, top). Indeed, blocking IL-6R completely reversed the phenotypic alterations imposed by chronic LCMV infection, as KLRG1 and IL-7Rα expression levels were comparable in LCMV-exposed and -unexposed memory bystander CD8+ T cells (Fig. 6 B). Of note, during chronic LCMV infection, a majority of bystander KLRG1+ OT-I T but not KLRG1- OT-I cells expressed high levels of IL-6Rα and ∼10% of IL-7Rα- memory OT-I cells already expressed IL-6Rα before LCMV infection (Fig. S5), and IL-7Rα- memory OT-I cells were shown to up-regulate KLRG1 during chronic LCMV infection (Fig. 4).

IL-6 blockade, however, did not affect the attrition of memory bystander cells (Fig. S4 F). To test whether IL-6 alone can induce the observed phenotypical changes, we injected 1 µg recombinant IL-6 (rIL-6) per day for 7 d into mice harboring memory OT-I CD8+ T cells (Fig. 6 C). Indeed, memory bystander T cells significantly up-regulated KLRG1 in the spleen and in the lung upon IL-6 treatment without infection, suggesting that IL-6 alone can alter the phenotype of memory bystander T cells. Next, we investigated whether IL-6 acts directly on the memory bystander T cells. We sorted memory OT-I T cells and cultured them in the presence of rIL-6 (Fig. 6 D). Memory OT-I T cells up-regulated KLRG1 in the presence of rIL-6.

Since IL-6 is also signaling via STAT1 and memory bystander T cells showed a strong ex vivo pSTAT1 signature upon chronic virus infection, we tested phenotypic alterations in CD8+ OT-I memory bystander T cells lacking STAT1. Therefore, we adoptively transferred equal numbers of memory CD8+ OT-I T cells with WT or Stat1-/- background into naive C57BL/6 recipients and infected these mice 1 d after transfer with a chronic dose of LCMV. Indeed, chronic virus infection did not induce phenotypic alterations toward an "effector-like" phenotype in Stat1-/- OT-I bystander T cells (Fig. 6 E). To corroborate that IL-6 signals via STAT1 in memory CD8+ T cells, we stained for pSTAT1 and pSTAT3 after 6 h of in vitro stimulation with rIL-6 and found that IL-6 signals via pSTAT1 in memory bystander T cells (Fig. 6 F). Together, these data suggest that high levels of IL-6 induced by chronic virus infection drive phenotypic alterations of memory bystander T cells in a direct, STAT1-dependent manner.

Chronic viral infection negatively impacts secondary expansion and protection of memory bystanders in a cell-extrinsic manner

Next, we analyzed whether a hallmark of memory CD8+ T cells, namely their rapid and pronounced recall response, was affected by chronic LCMV infection. Therefore, we transferred CD45.1+ OT-I CD8+ T cells into congenic CD45.2 WT C57BL/6 mice and induced memory OT-I CD8+ T cells by infection with recombinant vesicular stomatitis virus expressing OVA (VSV-OVA), followed by chronic LCMV infection 30 d after priming. 30 d after chronic LCMV infection, we challenged the memory bystander T cells with VV-OVA and analyzed the secondary expansion 8 d after VV-OVA challenge (Fig. 7 A). Strikingly, the memory bystander T cells that were exposed to chronic LCMV infection expanded to a much smaller extent than controls upon challenge with their cognate antigen (e.g., 18-fold less in the lung; Fig. 7 A). Since viral replication of VV-OVA was slightly reduced if the host was chronically LCMV infected (Fig. 7 C), we wanted to confirm these results by using a boosting strategy that would not rely on viral replication. To this end, we used SIIN-FEKL peptide combined with CpG as an adjuvant to challenge the bystander T cells and analyzed the expansion 8 d after challenge (Fig. 7 B). We could confirm that memory bystanders expanded to a much lower extent if exposed to a chronic virus infection. Upon peptide challenge, bystander CD8+ OT-I T cells even expanded 475-fold less than controls (Fig. 7 B). Next, we tested the protective capacity of memory bystander CD8+ T cells with and without exposure to chronic LCMV infection. To this end, mice were challenged with VV-OVA 30 d after LCMV infection and viral titers were quantified in ovaries 8 d after challenge (Fig. 7 C). We found that bystander T cells that had been exposed to a chronic virus infection conferred up to 3-log less protection compared with bystander T cells that had not been exposed to the chronic environment (Fig. 7 C).

To assess whether the reduced expansion potential of memory OT-I T cells in chronic LCMV-infected hosts was a result of cell-intrinsic or cell-extrinsic factors, we adoptively transferred memory bystander OT-I T cells that either had or had not been exposed to LCMV into naive hosts and challenged
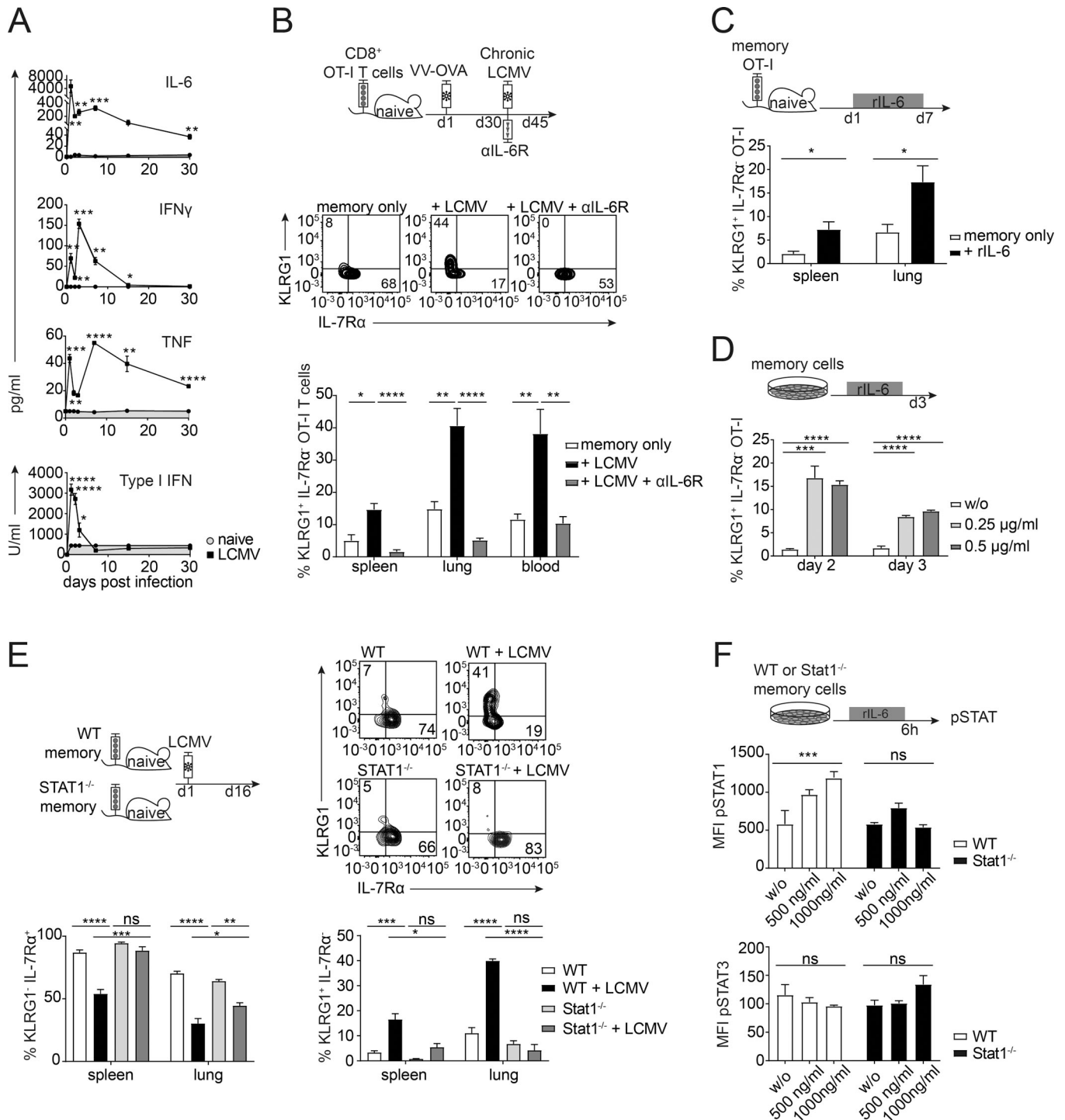
Barnstorf et al.
Bystander memory CD8 T cells in chronic infections

Journal of Experimental Medicine
https://doi.org/10.1084/jem.20181589

578

Figure 6. **IL-6 drives phenotypic alterations of memory bystander T cells. (A)** Cytokine levels in the serum over 30 d of infection (LCMV, open squares) and naive controls (naive, gray circles, gray area) were measured by CBA (IL-6, IFNγ, and TNF) or IFN bioassay (type I IFNs). **(B)** Top: Experimental approach. Adoptive transfer of CD45.1⁺ OT-I CD8⁺ T cells into congenic CD45.2 WT C57BL/6 mice, followed by priming with VV-OVA. On day 30 after priming, mice were persistently infected with LCMV docile. From the onset of the infection, αIL-6R blocking antibody was injected i.p. every second day. The experiment was terminated 15 d after LCMV infection. Middle: Representative flow cytometry plots of the expression of KLRG1 and IL-7Rα of memory only, + LCMV, and +LCMV + αIL-6R. Bottom: Quantification of percentages of KLRG1⁺ IL-7Rα⁻ OT-I T cells shown for memory only (white, uninfected) + LCMV (black), and +LCMV + αIL-6R (gray) in the spleen, lung, and blood. **(C)** Top: Experimental approach. Adoptive transfer of CD45.1⁺ OT-I CD8⁺ T cells into congenic CD45.2 WT C57BL/6 mice, followed by priming with VV-OVA. On day 30 after priming, mice were injected with 1 µg of rIL-6 every day for 1 wk. Bottom: Quantification of percentages of KLRG1⁺ IL-7Rα⁻ OT-I T cells shown for memory only (white, uninfected) and +rIL-6 (black) in the spleen and lung. **(D)** Top: Experimental approach. FACS-sorted memory OT-I CD8⁺ T cells were cultured in vitro with or without rIL-6 for 3 d. Bottom: Quantification of percentages of KLRG1⁺ OT-I T cells shown for no cytokine (w/o, white), 0.25 µg/ml (light gray), and 0.5 µg/ml (dark gray). **(E)** Top left: Experimental approach. Adoptive transfer of 5 × 10⁵ CD45.1⁺ WT memory OT-I or CD45.1⁺ *Stat1⁻/⁻* memory OT-I CD8⁺ T cells into congenic CD45.2⁺ WT C57BL/6 mice. 1 d after transfer, mice were persistently infected with

Barnstorf et al.
Bystander memory CD8 T cells in chronic infections

Journal of Experimental Medicine
579
https://doi.org/10.1084/jem.20181589

LCMV docile. The experiment was terminated 15 d after LCMV infection. Top right: Representative flow cytometry plots of the expression of KLRG1 and IL-7Rα for WT OT-I ± LCMV and *Stat1*−/− OT-I ± LCMV memory bystander T cells. Bottom: Quantification of percentages of KLRG1+ IL-7Rα− OT-I T cells and KLRG1− IL-7Rα+ OT-I T cells shown for WT (white, uninfected), WT + LCMV (black), *Stat1*−/− (light gray), and *Stat1*−/− + LCMV (dark gray) in the spleen and lung. **(F)** Experimental approach. FACS-sorted WT or *Stat1*−/− memory OT-I CD8 T cells were cultured in vitro with or without rIL-6 for 6 h. Bottom: Quantification of mean fluorescence intensity (MFI) of pSTAT1+ and pSTAT3+ WT (white) or Stat1−/− (black) OT-I T cells shown for no cytokine (w/o), 500 ng/ml, and 1000 ng/ml. One representative experiment out of two is shown with four to five mice per group (A–C and E) or triplicates for the in vitro experiments (D and F). Statistical analysis was performed using the unpaired two-tailed Student's *t* test: ns, $P \geq 0.05$; *, $P < 0.05$; **, $P < 0.01$; ***, $P < 0.001$; ****, $P < 0.0001$. Error bars show SEM.

these mice with VV-OVA. Surprisingly, the cells expanded to the same extent in spleen and lung, independent of their history (Fig. 7 D), indicating that the impaired secondary expansion within chronically infected hosts was due to cell-extrinsic factors. Since these extrinsic factors are likely associated with ongoing viral replication, we asked the question whether normal secondary expansion potential would be reached in chronically infected hosts after eventual control of LCMV infection. Therefore, we adoptively transferred CD45.1+ OT-I CD8 T cells into congenic CD45.2+ WT C57BL/6 mice, primed with VV-OVA and chronically infected with LCMV 30 d later. We performed longitudinal focus-forming assays from the blood of the chronically infected mice to determine when the mice controlled the infection. At 300 d after LCMV infection, no focus-forming units were detectable, and we analyzed the spleen and the lung for the phenotype of the memory bystander T cells. Interestingly, at this time point, IL-7Rα expression was restored to the same level as observed in LCMV uninfected mice. Additionally, KLRG1 expression was significantly decreased in these long-term bystanders but still slightly elevated compared with uninfected controls (Fig. 7 E).

These data show that viral clearance leads to partial reversion of the phenotypic alterations induced by chronic viral infection. To assess whether this also holds for the functional alterations, we performed in the same long-term experiment a challenge with SIINFEKL peptide and CpG-containing oligonucleotides as adjuvant once the chronic infection had resolved. Surprisingly, secondary expansion remained highly compromised in the spleen and in the lung, even though long-term memory bystander cells expanded slightly better in the lung compared with earlier time points of chronic infection (day 30; Fig. 7 F). These results suggest that, in addition to causing attrition of memory CD8 T cell numbers and skewing of the memory phenotype, chronic virus infection impacts markedly on the secondary expansion potential of memory bystander CD8+ T cells in a cell-extrinsic manner and thus severely hampers their protective capacity.

Discussion

While there is substantial knowledge about the impact of chronic viral infections on the regulation of virus-specific T cell immunity, much less is known about their influence on unrelated, heterologous T cell phenotypes and functions. We revealed a profound impact of chronic virus infections on existing heterologous immunity, focusing on memory bystander CD8+ T cells with specificity for OVA. Fully formed memory T cells were strongly reduced in total numbers in different organs,

which could be partly explained by the influence of perforin-mediated cytotoxicity of the virus-specific CD8+ T cells, leading to marked destruction of secondary lymphoid organ architecture and, in particular, possibly reduced IL-7–sensing opportunities. Previous studies have shown attrition of memory CD8+ T cells by heterologous virus infections, demonstrating that type I IFNs induced by the viral infection were driving apoptosis of bystander memory T cells during the early phase of infection (McNally et al., 2001; Jiang et al., 2005; Bahl et al., 2006). Still, it remained controversial whether this selective loss of memory bystanders was indeed due to active attrition as result of apoptosis or whether it was rather due to competition for niches between virus-specific and bystander cells, described as passive attrition (Welsh and Selin, 2009). There is clear evidence of virus-induced lymphopenia causing apoptosis and thereby reducing memory bystanders at the early stages of several viral infections (McNally et al., 2001; Peacock et al., 2003) and of type I IFNs causing apoptosis and the following forfeiture of CD44high CD8+ T cells (McNally et al., 2001). The survival of bystander memory T cells is based on the frequency of competing, newly generated memory cells, pursuant to the passive competition model. However, we show here that the loss of bystander T cells occurs already before virus-specific CD8+ T cells expand (Fig. S1 C) and is most pronounced upon chronic virus infection. Therefore, these observations favor the active deletion model, but more comprehensive research is needed to resolve this question (Kim and Welsh, 2004). Interestingly, not only type I IFNs but also type II IFNs (IFNγ) induce a durable loss of bystander memory CD8+ T cells upon challenge with intracellular bacteria, which has also been linked to active attrition rather than competition (Dudani et al., 2008). These studies indicate that memory attrition can be induced by type I and type II IFNs. We could also show that type I and type II IFNs were highly elevated early during chronic virus infection; nevertheless, their neutralization with the onset of chronic infection did not restore total numbers (Fig. S4).

Besides the loss of total numbers of memory bystander CD8+ T cells, we also revealed a pervasive effect of chronic virus infections on the phenotype and function of these T cells. These changes manifested toward a more exhausted-like phenotype and a reduced ability to produce effector cytokines. On a transcriptional level, LCMV-exposed bystander memory cells exhibited a signature that was closer to exhausted than effector T cells and also expressed higher levels of these markers on the protein level. IL-6 proved to be a major driver of these phenotypical changes in a T cell–intrinsic manner. Canonical memory CD8+ T cell properties, such as rapid secondary expansion, were severely reduced in the context of chronic bystander virus
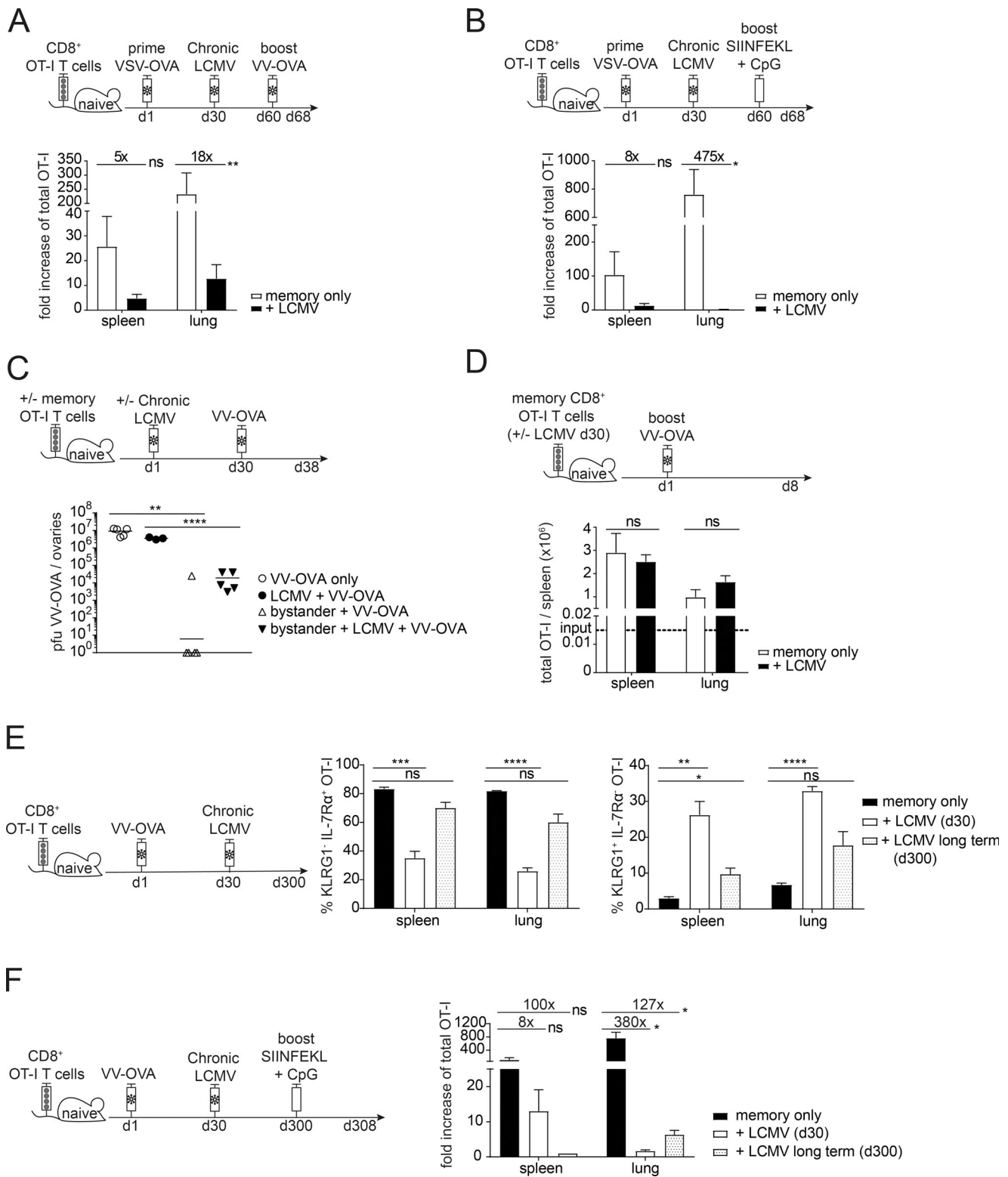
Figure 7. **Chronic viral infection negatively impacts secondary expansion and protection of memory bystanders in a cell-extrinsic manner. (A)** Top: Experimental approach. Adoptive transfer of 3 × 10^5 CD45.1$^+$ OT-I CD8$^+$ T cells into congenic CD45.2 WT C57BL/6 mice, followed by priming with VSV-OVA. On day 30 after priming, mice were persistently infected with LCMV docile. 30 d after LCMV infection mice were infected with VV-OVA. Memory bystanders were analyzed for expansion 8 d after VV-OVA challenge. Bottom: Quantification of fold increase of OT-I T cells shown for memory only (white, uninfected) and + LCMV (black) in the spleen and in the lung. **(B)** Top: Experimental approach. Adoptive transfer of CD45.1$^+$ OT-I CD8$^+$ T cells into congenic CD45.2 WT C57BL/6 mice, followed by priming with VV-OVA. On day 30 after priming, mice were persistently infected with LCMV docile. 30 d after LCMV infection a vaccination boost of 50 µg SIINFEKL peptide and 10 µg CpG was injected intravenously. Memory bystanders were analyzed for expansion 8 d after challenge. Bottom: Quantification of fold increase of OT-I T cells shown for memory only (white, uninfected) and + LCMV (black) in the spleen and in the lung. **(C)** Top:

Experimental approach. Adoptive transfer of 5 × 10^5 CD45.1$^+$ OT-I memory CD8$^+$ T cells into congenic CD45.2 WT C57BL/6 mice. 1 d after transfer, mice were persistently infected with LCMV docile; controls remained uninfected. 30 d after LCMV infection, mice were injected intravenously with VV-OVA. Further controls were WT C57BL/6 mice that were persistently infected with LCMV docile or were left uninfected as controls. VV-OVA titers were analyzed 8 d after VV-OVA infection in the ovaries. Bottom: Quantification of PFUs VV-OVA/ovaries shown for VV-OVA only (circles, white), LCMV + VV-OVA (circles, black), bystander + VV-OVA (triangle, white), and bystander + LCMV + VV-OVA (triangle, black). **(D)** Top: Experimental approach. Adoptive transfer of 10^3 CD45.1$^+$ OT-I memory CD8$^+$ T cells, which had or had not been exposed to chronic LCMV infection for 30 d, into congenic CD45.2 WT C57BL/6 mice. 1 d after transfer, mice were infected with VV-OVA. Memory bystanders were analyzed for expansion 8 d after challenge. Bottom: Quantification of total numbers of OT-I T cells shown for memory only (white, uninfected) and + LCMV (black) in the spleen and in the lung. **(E)** Left: Experimental approach. Adoptive transfer of CD45.1$^+$ OT-I CD8$^+$ T cells into congenic CD45.2 WT C57BL/6 mice, followed by priming with VV-OVA. On day 30 after priming, mice were persistently infected with LCMV docile. The experiment was terminated after viral clearance at day 300. Right: Quantification of percentages of KLRG1$^+$ IL-7Rα$^-$ and KLRG1$^-$ IL-7Rα$^+$ OT-I T cells shown for memory only (black, uninfected), + LCMV (day 30, white), and +LCMV long term (day 300, white with black dots) in the spleen and in the lung. **(F)** Left: Experimental approach. Adoptive transfer of CD45.1$^+$ OT-I CD8$^+$ T cells into congenic CD45.2 WT C57BL/6 mice, followed by priming with VV-OVA. On day 30 after priming, mice were persistently infected with LCMV docile. After viral clearance at day 300, a vaccination boost of 50 µg SIINFEKL peptide and 10 µg CpG was injected intravenously. As a control, day 30 LCMV mice were included. Memory bystanders were analyzed for expansion 8 d after challenge. Right: Quantification of fold increase of total OT-I T cells shown for memory only (black, uninfected), + LCMV (day 30, white), and + LCMV long-term (day 300, white with black dots) in the spleen and in the lung. **(A–F)** One representative experiment out of two is shown with three to five mice per group. Statistical analysis was performed using the unpaired two-tailed Student's t test: ns, $P \geq 0.05$; *, $P < 0.05$; **, $P < 0.01$; ***, $P < 0.001$; ****, $P < 0.0001$. Error bars show SEM.

infection. This impairment depended on cell-extrinsic cues in the chronically infected host and was reverted in a naive environment. Collectively, these observations suggest that chronic virus infections alter multiple features of memory bystander T cells. Changes are mainly caused by the destruction of secondary lymphoid organ architecture by virus-specific CD8$^+$ T cells (with respect to maintenance of memory T cell numbers) and by the sustained provision of a proinflammatory cytokine milieu (with respect to their phenotypical alterations). Our experiments furthermore ruled out a possible cross-reactivity between the OT-I TCR and LCMV antigens; treatment of OT-I T cells with LCMV antigens resulted neither in their activation nor in the up-regulation of gene expression profiles normally associated with TCR signaling.

Our results complement a previous report showing that chronic virus infection alters the transition from effector to memory bystander CD8$^+$ T cells (Stelekati et al., 2014) and, in addition, give mechanistic details into the molecular pathways regulating such bystander memory T cell attrition and attenuation. In agreement with our study, Stelekati et al. (2014) found reduced numbers of bystander CD8$^+$ T cells. They observed that attrition of CD8$^+$ T cells upon poly(I:C)-induced inflammation was largely due to direct type I IFN signaling on bystander CD8$^+$ T cells. However, in the context of chronic LCMV infection, direct type I IFN signaling on bystander CD8$^+$ T cells only played a minor role in their numeric reduction and impaired effector to memory transition. Our study confirms that sustained type I IFN signaling occurs during chronic LCMV infection, manifested by IFN-stimulated gene signatures and a directly ex vivo traceable phosphorylated STAT1 in bystander memory CD8$^+$ T cells. However, in agreement with the results reported by Stelekati et al. (2014), we observed that sustained type I IFN signaling did not induce key phenotypical alterations of bystander memory CD8$^+$ T cells during chronic LCMV infection, shown by the failure of IFNAR blockade to revert the infection-induced changes. Instead, IL-6 signaling via STAT1 proved to be a major driver of key phenotypical changes in bystander memory CD8$^+$ T cells.

IL-6R signaling is known to induce phosphorylation of both STAT1 and STAT3 in T cells; however, the activation state of T cells seems to determine whether STAT1 phosphorylation can occur (Teague et al., 2000). Besides signaling via STATs, IL-6 also engages the Ras–ERK and PI3K–mTOR pathways (Schaper and Rose-John, 2015). We have observed that LCMV-exposed memory bystander CD8 T cells signal via STAT1 when treated with IL-6, but we have not formally analyzed whether IL-6 also engages the Ras–ERK and PI3K–mTOR pathways in these cells. Based on our observation that (1) the robust ex vivo pSTAT1 signal in bystander memory cells is abrogated upon IFNAR blockade, (2) IFNAR blockade does not rescue the phenotypical alterations in memory bystander cells, and (3) STAT1 deficiency in bystander memory T cells prevents the phenotypic changes, we hypothesize that additional pathways involving other signaling intermediates than STAT1 are cooperating with STAT1 to mediate the phenotypical changes observed in bystander memory CD8 T cells in the setting of chronic LCMV infection, likely involving the Ras–ERK and PI3K–mTOR pathways.

In the context of chronic LCMV infection, IL-6 is produced in an early (days 1–3 after infection) and late phase (day 25 after infection), mostly by irradiation-resistant cells (Harker et al., 2011). Eventual control of an established chronic LCMV infection is critically dependent on IL-6, which induces the up-regulation of the transcriptional regulator Bcl-6 in virus-specific CD4$^+$ T cells. This supports Tfh differentiation in the late chronic virus infection and leads to an improved antibody and an escalated germinal center response. Accordingly, IL-6 has been suggested to indirectly reduce CD8$^+$ T cell exhaustion in late chronic LCMV infection via regulation of CD4$^+$ T cell differentiation toward Tfh cells and ensuing generation of virus-neutralizing antibodies (Harker et al., 2011; Wherry and Kurachi, 2015; Greczmiel et al., 2017). Our results indicate that the sustained IL-6 production during chronic LCMV infection also affects T cell phenotypes beyond antigen-specific T cells. We show that prolonged IL-6 exposure instructs a transition toward a more exhausted phenotype in established bystander memory CD8$^+$ T cells.

Our study highlights the substantial impact of chronic virus infections on already existing heterologous immunity, which could serve as a basis to optimize therapeutic strategies and

increases the knowledge of memory development and maintenance.

Materials and methods

Mice

WT C57BL/6J mice were purchased from Janvier Elevage. C57BL/6J (originally from Janvier Elevage), Maxi transgenic (CD45.1) mice expressing a TCR specific for MCMV peptide M38$_{316-323}$ (Torti et al., 2011), P14 transgenic (CD45.1) mice expressing a TCR specific for LCMV peptide gp33$_{33-41}$ (Pircher et al., 1990; Torti et al., 2011), PKOB$^{-/-}$ (Kägi et al., 1994), CD45.1 OT-I mice expressing a TCR specific for OVA$_{257-264}$ SIINFEKL peptide (Hogquist et al., 1994), CD45.1 OT-I Rag1$^{-/-}$, and CD45.1 OT-I Stat1$^{-/-}$ (the Stat1$^{-/-}$ mice were purchased from Charles River Laboratories and crossed to the CD45.1 OT-I line) were housed and bred under specific pathogen–free conditions at the ETH Phenomics Center Hönggerberg. All KO and transgenic mice strains were crossed on a C57BL/6 background for >10 generations. All mice were used between 6–12 wk of age and sex-matched within all experiments. All animal experiments were performed according to the institutional policies and Swiss federal regulations, and those were approved by the Cantonal Veterinary Office of Zürich (Animal experimentation permissions 228/2013, 166/2016).

Viruses, infections, and depletions

Recombinant MCMV lacking m157 (MCMVΔm157) was previously described and is referred to as MCMV in this study (Walton et al., 2008). MCMV strains were propagated on MEFs (Brune et al., 2001) or M2-10B4 cells (Zurbach et al., 2014), as previously described. Virus titers in organs were determined by standard plaque-forming assays on M2-10B4 cells, as previously described (Zurbach et al., 2014). Mice were intravenously infected with 10^6 PFU MCMV. LCMV isolates WE and docile were provided by Dr. R.M. Zinkernagel (University Hospital Zürich, Zürich, Switzerland) and were propagated at a low multiplicity of infection (MOI) on L929 fibroblast cells (WE) or Madin-Darby Canine Kidney endothelial cells (docile). Acute LCMV infection was induced by i.v. infection with 200 ffu LCMV-WE; chronic infection was induced by i.v. infection with 2 × 10^6 ffu LCMV docile. Recombinant VSV-OVA-GFP was kindly provided by Dorothee von Laer (Medical University Innsbruck, Innsbruck, Austria). VSV-OVA-GFP was plaque-purified as described elsewhere (Ebert et al., 2004). To generate virus stocks of VSV-OVA-GFP on BHK-21 cells, the cells were infected with MOI 0.01, and after 36 h virus was harvested. Virus supernatant was filtered (0.45 µm) to remove cell debris and subsequently concentrated via low-speed centrifugation using a 20% sucrose cushion. Virus titer was determined on confluent BHK-21 monolayers using plaque or 50% tissue culture infective dose (TCID$_{50}$) assay. Mice were infected intravenously with 2 × 10^6 PFU. Recombinant VV-OVA was grown on BSC40 cells at low multiplicity of infection. Mice were infected i.p. with 10^6 PFU.

For blockade of IL-6R, 660 µg αIL-6R (clone: 15A7; BioXCell) was injected i.p. 1 d prior and then every second day after infection for 2 wk. For blockade of IFNAR, 500 µg αIFNAR (clone:

MAR1-5A3; BioXCell) was injected i.p. at day –1, 0, and 1 and then 250 µg αIFNAR every second day after infection for 2 wk. For cytokine neutralization, 500 µg anti-IL-7 (M25), 200 µg anti-IL-2 (JES6-1A12), and 500 µg IFNγ (XMG1.1) were injected i.p. every third day with the onset of infection for 1 wk. To test the effect of rIL-6 on memory bystander T cells, 1 µg rIL-6 (recombinant human IL-6 [carrier-free]; BioLegend) was injected i.p. every day for 1 wk.

Virus loads

Virus loads of LCMV were determined in the kidney, liver, or blood, as described (Battegay et al., 1991). Virus loads of VV were determined on BSC40 cells after 24 h of incubation (Unger and Traktman, 2004).

Flow cytometry and lymphocyte stimulation

Cell surface stainings were performed on blood samples, which were obtained via the leg vein and lymphocytes isolated from spleens and lungs. Single-cell suspensions were obtained by mashing spleens through a metal mesh using a syringe plunger. Blood samples were taken in FACS buffer containing EDTA. For the preparation of cells from the lung, mice were anaesthetized with 260 µl ketamine/xylacine/acepromacine mixture (2 mg ketamine, 0.4 mg xylacine, 60 µg acepromacine in PBS) by i.p. injection, and the lungs were perfused via the right heart ventricle with ∼5 ml PBS to remove circulating blood. Cells present in the lung lumen were removed by repeated flushing of the lumen with 1 ml PBS. The lungs were cut into small pieces and digested 2 × 20 min at 37°C with complete RPMI containing 2.4 mg/ml collagenase type I (GIBCO BRL Invitrogen) and 0.2 mg/ml DNase I (Roche Diagnostics), and mononuclear cells were purified by gradient centrifugation over 30% Percoll. Complete RPMI consisted of RPMI (Invitrogen) with 10% FCS (Omnilab), 2 mM L-glutamine (Gibco), and 1% penicillin/streptomycin (Gibco).

Surface staining of the obtained cells was performed for 20 min at 4°C in PBS. All samples were treated in the following with 1 ml ACK lysis buffer for RBC lysis for 5 min at room temperature (RT). Cells were then fixed in PBS containing 1% paraformaldehyde (PFA). Cytokine expression was analyzed by intracellular staining in stimulated lymphocytes. CD8 T cells were stimulated with 1 µg/ml of SIINFEKL peptide for 6 h at 37°C in the presence of monensin A. Surface staining was performed for 20 min at 4°C followed by permeabilization of the cells with 500 µl of 2 × FACS BD Lysis Solution with 0.08% Tween20 for 10 min at RT. After a washing step, the intracellular staining for IFNγ, TNF, and IL-2 was performed for 30 min at RT in the dark. Samples were stored in PBS containing 1% PFA. pSTAT1 staining was performed on lymphocytes directly ex vivo without further stimulation. Surface staining was performed for 20 min at 4°C followed by fixation with 4% PFA for 12 min at 37°C. Cells were permeabilized with 90% methanol for 30 min on ice, and Fc block was performed in the following with perm buffer + 2% FBS and Fc block (1:100) for 10 min at RT. Intracellular staining of pSTAT1 was performed for 45 min in 1× permeabilization/wash buffer from eBioscience FoxP3 staining kit. Cell proliferation dye (eBioscience Cell Proliferation Dye eFluor 450) staining was

performed according to the manufacturer's protocol. Fluorophore-conjugated antibodies were purchased from BioLegend (Lucerna Chem AG), eBioscience (Thermo Fisher Scientific), or BD Biosciences. The following antibodies (clones) were used for flow cytometry: anti-CD8α (53–6.7), anti-CD45.1 (A20), anti-KLRG1 (2F1), anti-CD127 (A7R34), anti-pSTAT1 pY701 (4a), anti-PD-1 (J43), anti-CD39 (Duha59), anti-IFNγ (XMG1.2), anti-TNF (MP6-XT22), and anti-IL-2 (JES6-5H4). Live/Dead Fixable near-IR (Life Technologies) dead cell stain was used to exclude dead cells. Multiparametric flow cytometric analysis was performed using an LSRII flow cytometer (BD Biosciences) and FACSDiva software. Data were analyzed using FlowJo software (Tree Star).

Adoptive transfer experiments
CD8 T cells from naive OT-I mice were purified from splenocytes using anti-CD8α magnetic activated cell sorting beads (Miltenyi Biotech) according to the manufacturer's instructions. 3×10^5 OT-I CD8 T cells were adoptively transferred into recipient mice 1 d before infection. Memory subsets were generated in C57BL/6J mice and isolated ≥30 d after infection. OT-I memory cells from the spleen were sorted from donor mice using a BD FACSAria Sorter. Sorted memory OT-I T cells were transferred into new hosts, used for in vitro assays, or used to extract RNA.

Calculation of fold increase of memory bystander T cells upon challenge
CD45.1 TCR-transgenic, OVA$_{257-264}$-specific (OT-I) CD8$^+$ T cells were adoptively transferred into congenic CD45.2 WT C57BL/6 mice. Mice were primed with VV-OVA. At least 30 d after transfer, once an OVA-specific memory T cell pool had been established, mice were persistently infected with LCMV docile. 30 d after LCMV infection mice were either sacrificed or infected with VV-OVA or injected with SIINFEKL + CpG in order to boost memory bystander T cells. Total numbers of before and after boost were calculated for different organs. The fold increase was calculated by dividing the total cell count after boost by the mean of total count of bystanders before boost:

$$\frac{\text{\# bystanders after boost}}{\text{\# bystanders before boost}} = \text{fold increase of CD8}^+ \text{ OT} - \text{I T cells.}$$

In vitro culture of memory bystander T cells in the presence of rIL-6
CD45.1 TCR-transgenic, OVA$_{257-264}$-specific (OT-I) CD8$^+$ T cells were adoptively transferred into congenic CD45.2 WT C57BL/6 mice. Mice were primed with VV-OVA. At least 30 d after transfer, once an OVA-specific memory T cell pool had been established, mice were sacrificed and lymphocytes were isolated from the spleen as described before. Cell surface staining was performed with the following antibodies: anti-CD8α (53–6.7), anti-CD45.1 (A20). Cells were sorted for CD8$^+$ CD45.1$^+$ using a BD FACSAria Sorter. 10^5 sorted memory cells/well were cultured in T cell complete medium (RPMI 1640 [BioConcept], 2 mM L-glutamine [BioConcept], 2% penicillin/streptomycin [Sigma-Aldrich], 10% FCS [Gibco], 25 mM HEPES [Pan Biotech], 1× nonessential amino acids [Sigma], 50 μM β-mercaptoethanol

[Gibco], 1 mM sodium pyruvate [Gibco]) round-bottom 96-well plates. Cells were cultured in the presence of 100 ng/ml IL-7 (eBioscience) and 100 ng/ml IL-15 (eBioscience). Memory bystanders were either exposed to medium only or 0.25 μg/ml, 0.5 μg/ml, or 1 μg/ml of rIL-6 for 3 d or 6 h (recombinant mouse IL-6 [carrier-free]; BioLegend).

Immunohistochemistry and fluorescence microscopy
7-μm thin sections were prepared from frozen spleens embedded in optimal cutting temperature compound (Sakura). These sections were air-dried and afterwards fixed in 4% PFA for 30 min at RT. After a washing step, sections were incubated with blocking buffer (PBS + 10% FCS) for 1 h at RT. Staining was performed with the following antibodies (diluted 1:100 in PBS with 1% FCS, B220 was diluted 1:50) for 1 h at RT in the dark: anti-podoplanin (8.1.1), anti-CD45.1 (A20), anti-B220 (RA3-6B2), and anti-CD3 (17A2). Afterwards, slides were washed twice with PBS and once with water, followed by mounting with Mowiol (Sigma-Aldrich). 20–30 Z-stacks (1 μm) were acquired with a Visitron Confocal System (inverse confocal microscope; Visitron Systems GmbH) with 10× magnification (10× objective; type: Plan-Neofluar; aperture: 0.3; immersion: air; contrast: Ph1) at RT. Acquisition of fluorescence pictures was performed using Evolve 512 EMCCD cameras (Photometrics). Data were analyzed using Volocity software (version 6.3; PerkinElmer).

Illumina sequencing
After sorting, the cells were resuspended and frozen in TRI Reagent (Zymo Research). RNA was isolated using the Zymo Research Direct-zol RNA MicroPrep (R2060) according to the manufacturer's protocol. RNA-seq libraries were prepared using the SMARTer Stranded Total RNA-Seq Kit for Pico Input Mammalian from Clonetech. Briefly, total RNA samples (0.25–10 ng) were reverse-transcribed using random priming into double-stranded cDNA in the presence of a template switch oligo (TSO). When the reverse transcription reaches the 5′ end of the RNA fragment, the enzyme's terminal transferase activity adds nontemplated nucleotides to the 3′ end of the cDNA. The TSO pairs with the added nontemplated nucleotide, enabling the reverse transcription to continue replicating to the end of the oligonucleotide. This results in a cDNA fragment that contains sequences derived from the random priming oligo and the TSO. PCR amplification using primers binding to these sequences can now be performed. The PCR adds full-length Illumina adapters, including the index for multiplexing. Adapter sequences are shown in Table S1. Ribosomal cDNA is cleaved by ZapR in the presence of the mammalian-specific R-Probes. Remaining fragments are enriched with a second round of PCR amplification using primers designed to match Illumina adapters. The quality and quantity of the enriched libraries were validated using Qubit (1.0) Fluorometer and the Tapestation (Agilent). The product is a smear with an average fragment size of ~360 bp. The libraries were normalized to 10 nM in Tris-Cl 10 mM, pH 8.5, with 0.1% Tween 20.

The TruSeq SR Cluster Kit v4-cBot-HS or TruSeq PE Cluster Kit v4-cBot-HS (Illumina, Inc.) was used for cluster generation

using 8 pM of pooled normalized libraries on the cBOT. The libraries were sequenced on the Illumina HiSeq 2500 paired end at 2 × 126 bp or single end 126 bp using the TruSeq SBS Kit v4-HS (Illumina, Inc.). Read-alignment was performed using STAR (v2.5.3a) using the reference genome GRCm38.p5 and with the genome annotations from Ensembl (release 89). Gene expression values were computed using the function featureCounts from the R package Rsubread (v1.26.0) with the minimum quality mapping score set to 10 and the minimum feature overlap parameter set to 10 bp. Differential expression was computed using the generalized linear model implemented in the Bioconductor package EdgeR (v3.18.1) using trimmed mean of M values (TMM) as a normalization method.

RNA-seq data have been deposited in the ArrayExpress database at EMBL-EBI under accession no. E-MTAB-7594.

Statistical analysis

Statistical significance was determined as indicated by two-tailed Student's *t* test using GraphPad Prism. Statistical significance was determined with *, $P < 0.05$, **, $P < 0.01$, ***, $P < 0.001$, ****, $P < 0.0001$.

Online supplemental material

Fig. S1 shows the numeric reduction of bystander memory OT-I CD8^{+} T cells upon MCMV infection, quantification of bystander memory OT-I CD8^{+} T cells upon acute or chronic LCMV infection, longitudinal quantification of bystander memory OT-I CD8^{+} T cells upon chronic LCMV infection, quantification of bystander memory OT-I CD8^{+} T cells upon chronic LCMV infection in the presence or absence of NK cells, and quantification of memory OT-I CD8^{+} T cells in the presence or absence of LCMV-specific effector CD8^{+} T cells. Fig. S2 shows that OT-I CD8^{+} T cells do not recognize LCMV-derived antigens, phenotypic alterations of memory bystander OT-I CD8^{+} T cells upon exposure to acute or chronic LCMV infection, cytokine production by memory bystander OT-I CD8^{+} T cells in lung and quantification of memory bystander OT-I CD8^{+} T cells in spleen and lung, phenotypic alterations of memory bystander Rag1^{−/−} OT-I CD8^{+} T cells in spleen and lung upon chronic LCMV infection, PD-1 expression on memory bystander T cells in the spleen and in the lung, and PD-1 CD39 coexpression on memory bystander T cells in the spleen and in the lung. Fig. S3 shows RNA-seq analysis of memory bystander OT-I CD8^{+} T cells in the presence or absence of chronic LCMV infection. Fig. S4 shows ex vivo pSTAT1 expression in memory bystander OT-I CD8^{+} T cells, quantification and pSTAT1 expression of memory bystander OT-I CD8^{+} T cells upon IFNAR blockade, serum cytokine levels, phenotypic and numeric alterations of memory bystander OT-I CD8^{+} T cells upon chronic LCMV infection and IFNAR blockade, phenotypic and numeric alterations of memory bystander OT-I CD8^{+} T cells upon chronic LCMV infection and cytokine blockade, and numeric alterations of memory bystander OT-I CD8^{+} T cells upon chronic LCMV infection and IL-6R blockade. Fig. S5 shows IL-6R expression on memory bystander OT-I CD8^{+} T cells. Table S1 shows adapter sequences for Illumina sequencing.

References

Bahl, K., S.K. Kim, C. Calcagno, D. Ghersi, R. Puzone, F. Celada, L.K. Selin, and R.M. Welsh. 2006. IFN-induced attrition of CD8 T cells in the presence or absence of cognate antigen during the early stages of viral infections. *J. Immunol.* 176:4284–4295. https://doi.org/10.4049/jimmunol.176.7.4284

Bastidas, S., F. Graw, M.Z. Smith, H. Kuster, H.F. Günthard, and A. Oxenius. 2014. CD8+ T cells are activated in an antigen-independent manner in HIV-infected individuals. *J. Immunol.* 192:1732–1744. https://doi.org/10.4049/jimmunol.1302027

Battegay, M., S. Cooper, A. Althage, J. Bänziger, H. Hengartner, and R.M. Zinkernagel. 1991. Quantification of lymphocytic choriomeningitis virus with an immunological focus assay in 24- or 96-well plates. *J. Virol. Methods.* 33:191–198. https://doi.org/10.1016/0166-0934(91)90018-U

Beura, L.K., S.E. Hamilton, K. Bi, J.M. Schenkel, O.A. Odumade, K.A. Casey, E.A. Thompson, K.A. Fraser, P.C. Rosato, A. Filali-Mouhim, et al. 2016. Normalizing the environment recapitulates adult human immune traits in laboratory mice. *Nature.* 532:512–516. https://doi.org/10.1038/nature17655

Brune, W., H. Hengel, and U.H. Koszinowski. 2001. A mouse model for cytomegalovirus infection. *Curr. Protoc. Immunol.* Chapter 19:7. https://doi.org/10.1002/0471142735.im1907s43

Burton, D.R., P. Poignard, R.L. Stanfield, and I.A. Wilson. 2012. Broadly neutralizing antibodies present new prospects to counter highly antigenically diverse viruses. *Science.* 337:183–186. https://doi.org/10.1126/science.1225416

Cubas, R.A., J.C. Mudd, A.L. Savoye, M. Perreau, J. van Grevenynghe, T. Metcalf, E. Connick, A. Meditz, G.J. Freeman, G. Abesada-Terk Jr., et al. 2013. Inadequate T follicular cell help impairs B cell immunity during HIV infection. *Nat. Med.* 19:494–499. https://doi.org/10.1038/nm.3109

Doria-Rose, N.A., and M. Connors. 2009. Antibody-secreting B cells in HIV infection. *Curr. Opin. HIV AIDS.* 4:426–430. https://doi.org/10.1097/COH.0b013e32832d9fac

Dudani, R., K. Murali-Krishna, L. Krishnan, and S. Sad. 2008. IFN-gamma induces the erosion of preexisting CD8 T cell memory during infection with a heterologous intracellular bacterium. *J. Immunol.* 181:1700–1709. https://doi.org/10.4049/jimmunol.181.3.1700

Ebert, O., K. Shinozaki, C. Kournioti, M.S. Park, A. García-Sastre, and S.L. Woo. 2004. Syncytia induction enhances the oncolytic potential of vesicular stomatitis virus in virotherapy for cancer. *Cancer Res.* 64:3265–3270. https://doi.org/10.1158/0008-5472.CAN-03-3753

Fahey, L.M., E.B. Wilson, H. Elsaesser, C.D. Fistonich, D.B. McGavern, and D.G. Brooks. 2011. Viral persistence redirects CD4 T cell differentiation toward T follicular helper cells. *J. Exp. Med.* 208:987–999. https://doi.org/10.1084/jem.20101773

Frebel, H., K. Richter, and A. Oxenius. 2010. How chronic viral infections impact on antigen-specific T-cell responses. *Eur. J. Immunol.* 40:654–663. https://doi.org/10.1002/eji.200940102

Greczmiel, U., N.J. Kräutler, A. Pedrioli, I. Bartsch, P. Agnellini, G. Bedenikovic, J. Harker, K. Richter, and A. Oxenius. 2017. Sustained T follicular helper cell response is essential for control of chronic viral infection. *Sci. Immunol.* 2:1–12. https://doi.org/10.1126/sciimmunol.aam8686

Gupta, P.K., J. Godec, D. Wolski, E. Adland, K. Yates, K.E. Pauken, C. Cosgrove, C. Ledderose, W.G. Junger, S.C. Robson, et al. 2015. CD39 Expression Identifies Terminally Exhausted CD8+ T Cells. *PLoS Pathog.* 11:e1005177. https://doi.org/10.1371/journal.ppat.1005177

Hangartner, L., R.M. Zinkernagel, and H. Hengartner. 2006. Antiviral antibody responses: the two extremes of a wide spectrum. *Nat. Rev. Immunol.* 6:231–243. https://doi.org/10.1038/nri1783

Harker, J.A., G.M. Lewis, L. Mack, and E.I. Zuniga. 2011. Late interleukin-6 escalates T follicular helper cell responses and controls a chronic viral infection. *Science.* 334:825–829. https://doi.org/10.1126/science.1208421

Hogquist, K.A., S.C. Jameson, W.R. Heath, J.L. Howard, M.J. Bevan, and F.R. Carbone. 1994. T cell receptor antagonist peptides induce positive selection. *Cell.* 76:17–27. https://doi.org/10.1016/0092-8674(94)90169-4

Jiang, J., D. Gross, S. Nogusa, P. Elbaum, and D.M. Murasko. 2005. Depletion of T cells by type I interferon: differences between young and aged mice. *J. Immunol.* 175:1820–1826. https://doi.org/10.4049/jimmunol.175.3.1820

Kaech, S.M., and W. Cui. 2012. Transcriptional control of effector and memory CD8+ T cell differentiation. *Nat. Rev. Immunol.* 12:749–761. https://doi.org/10.1038/nri3307

Kägi, D., B. Ledermann, K. Bürki, P. Seiler, B. Odermatt, K.J. Olsen, E.R. Podack, R.M. Zinkernagel, and H. Hengartner. 1994. Cytotoxicity mediated by T cells and natural killer cells is greatly impaired in perforin-deficient mice. *Nature.* 369:31–37. https://doi.org/10.1038/369031a0

Kim, S.K., and R.M. Welsh. 2004. Comprehensive early and lasting loss of memory CD8 T cells and functional memory during acute and persistent viral infections. *J. Immunol.* 172:3139–3150. https://doi.org/10.4049/jimmunol.172.5.3139

Klenerman, P., and A. Oxenius. 2016. T cell responses to cytomegalovirus. *Nat. Rev. Immunol.* 16:367–377. https://doi.org/10.1038/nri.2016.38

McNally, J.M., C.C. Zarozinski, M.Y. Lin, M.A. Brehm, H.D. Chen, and R.M. Welsh. 2001. Attrition of bystander CD8 T cells during virus-induced T-cell and interferon responses. *J. Virol.* 75:5965–5976. https://doi.org/10.1128/JVI.75.13.5965-5976.2001

O'Hara, G.A., S.P. Welten, P. Klenerman, and R. Arens. 2012. Memory T cell inflation: understanding cause and effect. *Trends Immunol.* 33:84–90. https://doi.org/10.1016/j.it.2011.11.005

Peacock, C.D., S.K. Kim, and R.M. Welsh. 2003. Attrition of virus-specific memory CD8+ T cells during reconstitution of lymphopenic environments. *J. Immunol.* 171:655–663. https://doi.org/10.4049/jimmunol.171.2.655

Pircher, H., D. Moskophidis, U. Rohrer, K. Bürki, H. Hengartner, and R.M. Zinkernagel. 1990. Viral escape by selection of cytotoxic T cell-resistant virus variants in vivo. *Nature.* 346:629–633. https://doi.org/10.1038/346629a0

Reese, T.A., K. Bi, A. Kambal, A. Filali-Mouhim, L.K. Beura, M.C. Bürger, B. Pulendran, R.P. Sekaly, S.C. Jameson, D. Masopust, et al. 2016. Sequential Infection with Common Pathogens Promotes Human-like Immune Gene Expression and Altered Vaccine Response. *Cell Host Microbe.* 19:713–719. https://doi.org/10.1016/j.chom.2016.04.003

Sarkar, S., V. Kalia, W.N. Haining, B.T. Konieczny, S. Subramaniam, and R. Ahmed. 2008. Functional and genomic profiling of effector CD8 T cell subsets with distinct memory fates. *J. Exp. Med.* 205:625–640. https://doi.org/10.1084/jem.20071641

Schaper, F., and S. Rose-John. 2015. Interleukin-6: Biology, signaling and strategies of blockade. *Cytokine Growth Factor Rev.* 26:475–487. https://doi.org/10.1016/j.cytogfr.2015.07.004

Snyder, C.M. 2011. Buffered memory: a hypothesis for the maintenance of functional, virus-specific CD8(+) T cells during cytomegalovirus infection. *Immunol. Res.* 51:195–204. https://doi.org/10.1007/s12026-011-8251-9

Stelekati, E., H. Shin, T.A. Doering, D.V. Dolfi, C.G. Ziegler, D.P. Beiting, L. Dawson, J. Liboon, D. Wolski, M.A. Ali, et al. 2014. Bystander chronic infection negatively impacts development of CD8(+) T cell memory. *Immunity.* 40:801–813. https://doi.org/10.1016/j.immuni.2014.04.010

Teague, T.K., B.C. Schaefer, D. Hildeman, J. Bender, T. Mitchell, J.W. Kappler, and P. Marrack. 2000. Activation-induced inhibition of interleukin 6-mediated T cell survival and signal transducer and activator of transcription 1 signaling. *J. Exp. Med.* 191:915–926. https://doi.org/10.1084/jem.191.6.915

Torti, N., S.M. Walton, T. Brocker, T. Rülicke, and A. Oxenius. 2011. Non-hematopoietic cells in lymph nodes drive memory CD8 T cell inflation during murine cytomegalovirus infection. *PLoS Pathog.* 7:e1002313. https://doi.org/10.1371/journal.ppat.1002313

Unger, B., and P. Traktman. 2004. Vaccinia virus morphogenesis: a13 phosphoprotein is required for assembly of mature virions. *J. Virol.* 78:8885–8901. https://doi.org/10.1128/JVI.78.16.8885-8901.2004

Virgin, H.W., E.J. Wherry, and R. Ahmed. 2009. Redefining chronic viral infection. *Cell.* 138:30–50. https://doi.org/10.1016/j.cell.2009.06.036

Walton, S.M., P. Wyrsch, M.W. Munks, A. Zimmermann, H. Hengel, A.B. Hill, and A. Oxenius. 2008. The dynamics of mouse cytomegalovirus-specific CD4 T cell responses during acute and latent infection. *J. Immunol.* 181:1128–1134. https://doi.org/10.4049/jimmunol.181.2.1128

Welsh, R.M., and L.K. Selin. 2009. Attrition of memory CD8 T cells. *Nature.* 459:E3–E4, discussion :E4. https://doi.org/10.1038/nature08091

Wherry, E.J. 2011. T cell exhaustion. *Nat. Immunol.* 12:492–499. https://doi.org/10.1038/ni.2035

Wherry, E.J., and M. Kurachi. 2015. Molecular and cellular insights into T cell exhaustion. *Nat. Rev. Immunol.* 15:486–499. https://doi.org/10.1038/nri3862

Wherry, E.J., S.J. Ha, S.M. Kaech, W.N. Haining, S. Sarkar, V. Kalia, S. Subramaniam, J.N. Blattman, D.L. Barber, and R. Ahmed. 2007. Molecular signature of CD8+ T cell exhaustion during chronic viral infection. *Immunity.* 27:670–684. https://doi.org/10.1016/j.immuni.2007.09.006

Zurbach, K.A., T. Moghbeli, and C.M. Snyder. 2014. Resolving the titer of murine cytomegalovirus by plaque assay using the M2-10B4 cell line and a low viscosity overlay. *Virol. J.* 11:71–71. https://doi.org/10.1186/1743-422X-11-71